Cross section measurements for the neutron inelastic scattering and the (n, $2n\gamma$) reaction on ^{206}Pb

A. Negret,[1,*] L.C. Mihailescu,[2] C. Borcea,[1] Ph. Dessagne,[3,4] K.H. Guber,[5] M. Kerveno,[3,4] A.J. Koning,[6] A. Olacel,[1,7] A.J.M. Plompen,[8] C. Rouki,[8] and G. Rudolf[3,4]

[1] *"Horia Hulubei" National Institute for Physics and Nuclear Engineering, 077125 Bucharest-Măgurele, Romania*
[2] *Studiecentrum voor Kernenergie - Centre d'Etude de l'Energie Nucleaire, B-2400 Mol, Belgium*
[3] *Université de Strasbourg, IPHC, 67037 Strasbourg, France*
[4] *CNRS, UMR7178, 67037 Strasbourg, France*
[5] *Nuclear Science and Technology Division, Oak Ridge National Laboratory, Oak Ridge, TN 37831, United States*
[6] *Nuclear Research Group Petten, 1755 ZG Petten, The Netherlands*
[7] *University of Bucharest, Faculty of Physics, 077125, Bucharest-Măgurele, Romania*
[8] *European Commission, Joint Research Centre, Institute for Reference Materials and Measurements, B-2440 Geel, Belgium*

(Dated: May 6, 2015)

Excitation functions for γ production associated with the neutron inelastic scattering and the (n, $2n$) reactions on ^{206}Pb were measured from threshold up to about 18 MeV for about 40 transitions. Two independent measurements were performed using different samples and acquisition systems in order to check consistency of the results. The neutron flux was determined with a ^{235}U fission chamber and a procedure that were validated against a fluence standard. For incident energy higher than the threshold for the first excited level and up to 3.5 MeV, estimates are provided for the total inelastic and level cross sections by combining the present γ production cross sections with the level and decay data of ^{206}Pb reported in the literature. The uncertainty common to all incident energies is 3.0% allowing overall uncertainties from 3.3 to 30% depending on transition and neutron energy. The present data agree well with earlier work, but significantly expand the experimental database while comparisons with model calculations using the TALYS reaction code show good agreement over the full energy range.

PACS numbers: 25.40.Fq, 29.30.Kv, 27.80.+w, 24.10.-i

I. INTRODUCTION

Nuclear data with low uncertainties are needed for the design of the future generation of nuclear facilities (Generation-IV reactors and Accelerator Driven Systems - ADS). Lead is considered for the cooling system of such reactors. Sensitivity studies for ADS [1] showed that the required uncertainty for inelastic scattering cross sections of lead isotopes below 20 MeV is about 10%, while for the (n, $2n$) reaction it is of the order of 20%. For lead-cooled fast reactors a similar sensitivity study resulted in a required uncertainty of about 5% for inelastic scattering cross sections of ^{206}Pb for an incident neutron energy below 6 MeV [2]. Those sensitivity studies propagate nuclear data uncertainties to determine the uncertainties on estimates of key reactor parameters (effective multiplication factor, power peak, coolant void and temperature reactivity coefficients, change of reactivity from beginning to end of the fuel cycle). Required nuclear data uncertainties follow from the constraints imposed by the target uncertainties on such estimates. The tighter requirements from the lead-cooled fast reactor are largely due to the use of more stringent uncertainty requirements imposed on these reactor parameters. With similar tight requirements for an ADS the required uncertainty for the ^{206}Pb inelastic scattering cross section becomes 3-4% [3]. The accuracy of the inelastic scattering cross section is essential because the process represents the dominant mechanism for energy loss in the systems where light elements and particularly hydrogen are absent.

Neutron inelastic and (n, $2n$) data for ^{206}Pb of the required accuracy and completeness are a challenge both experimentally and theoretically. Experimentally the required accuracy is within reach but only for part of the required data. Theoretical models can provide the full range of cross sections, emitted particle spectra and angular distributions but lack the accuracy. While the main motivation for the present investigation comes from the tight demands set by applications, it is absolutely necessary to use a judicious combination of extremely precise experimental techniques and state-of-the-art model calculations in order to achieve the goal.

Neutron inelastic scattering cross sections for ^{206}Pb were previously measured using either the (n, n') technique, i.e. by detection of the outgoing neutrons, or the (n, $n'\gamma$) technique detecting the associated γ rays. Measurements with the first technique [4–9] were performed at energies between 2 MeV and 8 MeV. These experiments measured the differential cross sections for the first excited levels or determined level density parameters from the emission spectra [7, 10]. The (n, $n'\gamma$) technique was used in references [11–17] either with Ge(Li) or with NaI detectors. Most of these works used radiogenic samples with about 88% ^{206}Pb. Concerning the

*Email: alnegret@tandem.nipne.ro

^{206}Pb$(n, 2n)$ reaction, Jönsson *et al.* [13] determined a γ production cross section for the 987.7-keV transition of ^{205}Pb, Salaita and Eapen [18] and Garg and Khurana [19] determined isomeric cross sections by the activation technique while Fréhaut et al. [20] determined the total $(n, 2n)$ cross section by counting the emitted neutrons. Important complementary data for modeling and a discussion of the non-elastic cross section of ^{206}Pb are those for the total cross section [4, 21–28] and the elastic scattering angular distribution and cross section [29–35].

Here we primarily aim at providing a new large data set for inelastic scattering with the best achievable accuracy for the cross section and the highest achievable resolution for the incident energy.

A new experiment was performed at the GELINA (Geel Linear Accelerator) neutron time of flight facility to significantly improve the knowledge on the neutron inelastic and $(n,\ 2n\gamma)$ cross sections for ^{206}Pb below 20 MeV. The $(n,\ xn\gamma)$ technique was used. The γ rays from the ^{206}Pb$(n,$ x$n\gamma)$ reaction (x=1 and 2) were detected with four large volume HPGe (high-purity germanium) detectors. The high energy resolution of the germanium detectors allowed clear identification of the γ rays. A precise angle integration was possible placing the detectors at 110° and 150° with respect to the neutron beam direction. The full energy range from threshold up to about 20 MeV was covered with a neutron energy resolution of 1.3 keV at 1 MeV (42 keV at 10 MeV) for the strongest γ rays. The measured cross sections were normalized to the standard ^{235}U(n,f) cross section [36] using a new procedure that was validated by an inter comparison with reference fluence measurement instruments of Physikalisch Technische Bundesaustalt. Two independent measurements were performed using different acquisition systems and different samples. The results of the two measurements agree very well increasing the confidence in the results.

At least one γ ray was observed from the decay of the levels up to 2236.5 keV with the exception of the $J^{\pi}=0^{+}$ level at 1166.4 keV and the 180-μs isomer at 2200.2-keV excitation energy. Above 2236.5 keV, for more and more levels a decaying γ ray was not observed, the maximum excitation energy of a level with an observed decay being 3606.2 keV. The γ production cross section was measured for 34 γ rays from the inelastic channel. Two γ rays from the ^{206}Pb$(n,\ 2n\gamma)^{205}$Pb reaction were also observed: 703.4 keV and 987.6 keV. No γ rays from the first two excited levels of the ^{205}Pb nucleus were observed due to their low energy.

For the ^{206}Pb nucleus there are two major limitations in the use of the $(n,\ n'\gamma)$ technique in addition to the inherent limitation that no information is obtained about the scattered neutron's angular distribution. The first one is the presence of an E0 transition that dominates the decay of second excited level at 1166.4 keV ($J^{\pi}=0^{+}$) to the ground state [37]. This transition is fully converted internally and therefore it cannot be observed with HPGe detectors. The γ decay of the 0^{+} level to the first excited level is so weak that it could not be observed by us nor in earlier work. The second limitation concerns an isomer at 2200.2 keV with a lifetime of 180(3) μs [37]. The γ rays from the decay of this isomer (516.2 keV and 202.4 keV) are delayed and almost all of the decay occurs outside of the 24-μs time span of the present measurement. Therefore the γ rays emitted following the decay of the isomer are hard to observe and in practice, no measurable yield was found below the inelastic threshold for a transition associated with its decay (e.g. the 881.0-keV γ ray that occurs after the 516.2-keV transition of the isomer). With these limitations in mind we constructed total and level inelastic cross sections based on the γ production data and the adopted level and decay scheme [37].

In order to investigate the status of modeling we compare this new data set with state of the art calculations using both a fully phenomenological approach and a microscopic approach. The phenomenological approach uses parameters optimized globally [38–41]. The microscopic approach uses optical model parameters, strength functions and level densities calculated on the basis of effective nuclear interactions and combinatorics [41–45]. In both cases version 1.6 of the TALYS reaction code was used [46, 47].

II. EXPERIMENTAL SETUP AND DATA ANALYSIS

Detailed descriptions of the experimental setup and data analysis were given in references [48–50]. Here, we focus on describing the specific points of the present experiment and refer to those references for further details.

A. Experimental setup

The measurements were performed at the GELINA neutron time of flight facility of EC-JRC-IRMM (European Commission - Joint Research Center - Institute for Reference Materials and Measurements). An electron linear accelerator produces 1-ns pulses with a mean energy of 100 MeV at a repetition rate of 800 Hz. The average current is ≈7 μA. The electrons impinge on a rotary depleted Uranium target producing bremsstrahlung. The white neutron spectrum with energies between 800 keV and 18 MeV from (γ,xn) and (γ,F) reactions is used. A detailed description of the facility can be found in Refs. [51–53].

Two measurements were carried out in which the γ rays emitted in the $(n, xn\gamma)$ reactions were detected using HPGe detectors. The main one labeled here as "This work 1" uses a large radiogenic lead sample and a fast digitizer-based data acquisition system. The second one ("This work 2") uses a highly enriched smaller lead sample and classical electronics and data acquisition. Table I gives the details about the samples. The radiogenic Pb was characterized by isotope mass spectrometry at

TABLE I: Sample characteristics for the two measurements. Sample mass, diameter (d), thickness (t) and isotope amount fractions are given (atom %). Uncertainties represent one standard deviation, throughout this work.

Measurement	mass (g)	d (mm)	t (mm)	^{204}Pb (%)	^{206}Pb (%)	^{207}Pb (%)	^{208}Pb (%)
This work 1 (natural sample)	215.48(1)	69.8(1)	5.01(1)	0.0749(3)	88.59(3)	8.46(4)	2.87(2)
This work 2 (enriched sample)	43.2781(7)	50.0(2)	2.02(4)	<0.01	99.82(3)	0.16(2)	0.02(1)

IRMM (see below), while the amount fractions for the enriched sample were provided by the Oak Ridge National Laboratory's Isotope Office, from which the material was borrowed. Each measurement used four detectors but two of those used in the first measurement were replaced by two others in the second one. The relative efficiencies of the detectors ranged from 95% to 100% in "This work 1" and from 76% to 105% in "This work 2". The two measurements allow for a careful check of the methods of data taking and data analysis and have served to commission a new digitizer-based data acquisition system.

The sample was positioned at a distance of 198.551 m from the neutron source and the beam was collimated to 61 mm. The distance between the sample and the front of the detectors ranged between 13.6 cm and 14.7 cm. In both experiments two detectors were placed at 110° and two at 150° so that a weighted sum of the differential cross sections at these two angles provided an accurate angle-integrated cross section for transitions with multipolarity up to 3 by the principle of Gauss-quadrature [48].

Data acquisition in "This work 1" involved 2 DC440 Aquiris digitizer cards (420 million samples per second, 12 bits sampling resolution) with 2 inputs each. These were controlled by a PC that processed the waveforms to obtain the time and amplitude of the registered events and stored these in list files. A separate trigger generated when a neutron-induced event occurs is provided to each card. The trigger time is determined by the arrival time of the electron burst at the neutron producing target. The acquired waveforms ranged from a microsecond before arrival of the γ flash due to the bremsstrahlung from the neutron target to a few microseconds after the time of flight for the lowest neutron energy of interest (i.e. the time of flight of ≈800-keV neutrons). A detailed description of the processing algorithms, tests and performances of the acquisition system was presented in Ref. [50]. Data acquisition in "This work 2" is based on classical electronics as described in Refs. [48, 49].

The neutron flux was permanently monitored using a multi-layer fission chamber with 3.066(6) mg/cm^2 of ^{235}U evenly distributed over 8 deposits. The active diameter (70 mm) of the fission chamber was larger than the beam diameter. The fission chamber was placed at 197.214 m from the neutron source, in the vicinity of the sample.

B. Data analysis

Raw data were sorted into time of flight versus pulse height matrices. Time of flight bins of 9.5 ns for "This work 1" and 8 ns for "This work 2" were used resulting in a resolution of 1.3 keV at 1 MeV and 42 keV at 10 MeV for "This work 1" (1.1 and 35 keV, respectively for "This work 2"). For lower yields (depending on transition and neutron energy) the bin sizes were increased in order to obtain a reasonable number of counts per bin.

The photopeak efficiency of the HPGe detectors was measured using point-like sources placed in the sample position. The measured efficiencies were corrected for the extended volume and for the self attenuation of the γ rays in the sample. These corrections were performed by means of simulations using the MCNP [54] code. The total uncertainty on the HPGe efficiency was between 1.7% and 2.1% up to 1.4 MeV γ-ray energy and about 4.5% for the γ rays with energy higher than 1.4 MeV. The uncertainty of the activity of the ^{152}Eu calibration source was 0.7%. The main contribution to the uncertainty is due to the Monte Carlo model of the setup [55].

The γ-production cross sections for the ^{206}Pb(n, $n'\gamma$)^{206}Pb reaction were also corrected for the attenuation and multiple scattering of the neutrons in the sample using MCNP simulations. For the most intense γ ray (803.1 keV), this correction is smaller than 1.5% below E$_n$=8.1 MeV and it increases fast above this energy due to the opening of the (n, 2n) channel. At 18 MeV it reaches about 50%. For the other transitions the reaction threshold increases and above 8.1 MeV the correction for the neutron attenuation and multiple scattering is smaller (less than 10% for all γ rays). The statistical uncertainties of the MCNP simulations were negligible.

Due to the high content in ^{207}Pb of the radiogenic sample (8.5%) of "This work 1", corrections were required for the contribution of the ^{207}Pb(n, 2$n\gamma$) reaction to the γ productions cross sections from the ^{206}Pb(n,nγ) reaction. These were performed for the two strongest inelastic transitions (803.1 keV and 537.5 keV) using the ^{207}Pb(n, 2$n\gamma$) cross sections reported in Ref. [56].

The ^{235}U(n, f) cross section of Ref. [36] was used to normalize the cross sections presented here. It should be noted that our current method for determining the fission chamber efficiency differs significantly from that pub-

lished earlier [48] and the resulting estimate is notably different. The new value for the efficiency of detecting a fission event is 0.861(10). This is about 12% lower than the value in Ref. [48] and results in higher cross sections than reported in Ref. [56]. The new method for determining this efficiency was validated by comparison with a recoil proton telescope, a ^{235}U fission chamber, a ^{238}U fission chamber and a NE213 liquid scintillator at the Physikalisch-Technische Bundesanstalt (PTB) [57–59].

The total inelastic and the level cross sections were constructed using the angle integrated γ production cross sections and the evaluated level scheme of ^{206}Pb [37] as it is described in Refs. [48, 49].

For several excited levels in ^{206}Pb the γ production cross section was measured for more than one γ ray. In these cases the branching ratios were also determined.

III. REACTION CALCULATIONS WITH TALYS 1.6

TALYS [60] is a well-known software used both for the analysis of reaction experiments and for generating nuclear data [47]. The main advantage of the code resides in its completeness: it implements in a unified approach various reaction mechanisms (direct, compound, multistep and fission processes) integrating ECIS-06 code [61] as a routine used for optical model and coupled-channels calculations. The default optical model parameters used by TALYS are those from Ref. [38]. The multi-step processes (preequilibrium) are described in the exciton model [39]. TALYS can be used over a very wide energy range (1 keV - 200 MeV) for target nuclei with the mass number A = 12-339.

An interesting feature of the code is the possibility to perform a reasonable calculation using only default parameters. Based on a global analysis of the available data [38–40, 42–46] TALYS provides default values for practically all input parameters required and, based on this feature, the code claims very strong predictive power.

The structure of ^{206}Pb at low excitation energies is described by two neutron holes in the double-magic nucleus (^{208}Pb). In order to describe the ^{206}Pb(n, x$n\gamma$) reactions TALYS employs the optical model together with DWBA and the multi-step theory. The threshold for the inelastic reaction is E_{th}^{inel}=807.0 keV. Immediately after the threshold the inelastic cross section is dominated by the compound nucleus mechanism. As the energy of the incoming neutron increases, the direct and preequilibrium mechanisms play a more important role while various inelastic channels open. The threshold of the ^{206}Pb(n, $2n$)^{205}Pb reaction is $E_{th}^{(n,2n)}$=8126.3 keV.

For a proper comparison with the experimental data, two corrections are necessary for the production cross section of the 803.1 keV γ ray (as well as for other transitions) given by the TALYS calculation. The first one regards the presence of an isomeric level at 2200.2 keV. The TALYS code neglects the long life time of this level and the γ rays from the isomer are considered as prompt transitions. For the comparison with the present measurement, the cross section of the γ rays that decay from the isomer (516.2 keV and 202.4 keV) has to be subtracted from the cross section of all the γ rays that are fed by the isomer.

The second correction regards the presence of the E0 transition. The TALYS code attributes the full decay strength of the 1166.4-keV, 0^+ level to the 363.3-keV transition that feeds the first excited level. This is contrary to the information in the latest evaluated level scheme [37], where the 363.3-keV transition has negligible intensity (less than 0.24%). Therefore the calculated γ production cross section of the 363.3 keV transition has to be subtracted from the calculated γ production cross section of the 803.1 keV in order to make a correct comparison. In practice, both corrections were performed by altering the structure files used by TALYS.

IV. RESULTS AND DISCUSSION

The experimental results obtained with both measured samples are presented below. The γ production cross section is shown in Sec. IV A for all observed transitions together with examples of differential γ production cross sections at 110° and 150°. For several excited levels in ^{206}Pb, at least two γ-rays were observed and the branching ratios were determined. The total inelastic and the level cross sections are given in section IV B.

A. γ production cross sections

Table II lists all known levels and transitions from ^{206}Pb according to the evaluated level scheme [37]. The levels and γs for which we determined the production cross sections are emphasized with bold characters. Some γ transitions were observed only in the first measurement where the statistics was slightly better. Fig. 1 shows an example of the amplitude spectrum obtained with one of the HPGe detectors and the ^{nat}Pb sample. The main peaks from the ^{206}Pb(n, $n'\gamma$)^{206}Pb reaction are marked.

1. The 803.1-keV transition

In ^{206}Pb the transition from the first excited level to the ground state is by far the most intense in the spectrum. The 803.1-keV γ ray is an E2 transition from the initial 2^+ level to the 0^+ ground state. A clear angle dependence of the differential γ production cross section was observed (Fig. 2). The ratio between the differential cross section at 110° and 150° has a minimum just above the inelastic threshold and it increases at higher energies becoming almost 1 for $E_n \geq$10 MeV. This trend is confirmed by a calculation with the CINDY code [62].

TABLE II: Low excitation levels and γ transitions in ^{206}Pb. All energy, spin and parity and branching ratio values are from the evaluated level scheme [37]. The levels and γs for which we determined the production cross sections are emphasized with bold characters.

E_L (keV)	J^π	E_γ (keV)	Branching ratio (%)	Final level		Notes
803.1	2^+	**803.1**[a]	100	0	0^+	
1166.4	0^+	363.3	≤0.24	803.1	2^+	Very weak, not observed
		1166.4		0	0^+	E0, completely converted
1340.5	3^+	**537.5**	100	803.1	2^+	
1466.8	2^+	126.4	3.8(4)	1340.5	3^+	
		663.8	100(1)	803.1	2^+	
		1466.8[a]	30.4(7)	0	0^+	
1684.0	4^+	**343.5**	35.4(5)	1340.5	3^+	
		881.0	100(1)	803.1	2^+	
1704.5	1^+	**1704.5**[a]	100	0	0^+	
1784.1	2^+	317.5	23(3)	1466.8	2^+	
		617.6	11(3)	1166.4	0^+	
		981.0[a]	100(4)	803.1	2^+	
		1784.7	5.2(15)	0	0^+	
1997.7	4^+	313.7	21(2)	1684.0	4^+	
		657.2	100(2)	1340.5	3^+	
		1194.7	14.5(8)	803.1	2^+	
2149.0	2^+	682.3	20(3)	1466.8	2^+	
		808.6	20(3)	1340.5	3^+	
		1345.9	100(5)	803.1	2^+	
2196.7	$(3)^+$	729.2	7(3)	1466.8	2^+	
		856.6	100	1340.5	3^+	
		1393.8	78(5)	803.1	2^+	
2200.2	7^-	202.4	0.11(1)	1997.7	4^+	Isomer, $T_{1/2}$=125 μs
		516.2	100(1)	1684.0	4^+	Not observed
2236.5		**1433.5**[b]	100	803.1	2^+	
2314	0^+					
2384.2	6^-	184.0	100	2200.2	7^-	
2391.3		**1588.2**	100	803.1	2^+	γ not separated from the 1588.6-keV γ ray
2423.4	2^+	639.0	4.9(13)	1784.1	2^+	
		718.9	48.5(20)	1704.5	1^+	
		956.6[b]	20.6(16)	1466.8	2^+	
		1082.7	8.5(16)	1340.5	3^+	
		1620.3	100(4)	803.1	2^+	
2647.8	3^-	964.2	6.4(7)	1684.0	4^+	
		1844.5	100(4)	803.1	2^+	
2658.3	9^-	458.1	100	2200.2	7^-	
2782.2	5^-	**398.0**	79.6(7)	2384.2	6^-	
		582.0	3.59(18)	2200.2	7^-	
		784.6	3.97(7)	1997.7	4^+	
		1098.3	100(11)	1684.0	4^+	
2826.3	$(4)^+$	44.1	6.4(8)	2782.2	5^-	
		434.9	20.5(18)	2391.3		
		442.1	34(4)	2384.2	6^-	
		1142.4[b]	100(4)	1684.0	4^+	
		2022.8	11.6(18)	803.1	2^+	
2864.6	7^-	480.4	91(9)	2384.2	6^-	
		664.2	100(5)	2200.2	7^-	
		1180.7[b]	68(7)	1684.0	4^+	
2929.1	4^+	**1588.6**	100	1340.5	3^+	γ not separated from the 1588.2-keV γ ray
2939.6	6^-	157.5	22.6(25)	2782.2	5^-	
		555.3	23.9(25)	2384.2	6^-	
		739.2	100(5)	2200.2	7^-	
2954.5	8^-	296.2	68(8)	2658.3	9^-	
		754.4	100(8)	2200.2	7^-	
2960						
2984	2^+					
3016.4	5^-	190.0	22.6(25)	2826.3	$(4)^-$	
		234.2	5.4(3)	2782.2	5^-	
		632.3	100(1)	2384.2	6^-	
		816.3		2200.2	7^-	
		1332.3	6.3(3)	1684.0	4^+	
3033						
3122.4	(3^+)	1655.5	28(7)	1466.8	2^+	
		2319.3[b]	100(10)	803.1	2^+	
3139						
3194	(5^-)					
3194.3	(1,2)	2391.0	65(15)	803.1	2^+	
		3194.6	100(19)	0	0^+	
3225.4	$(5,6,7)^-$	360.8		2864.6	7^-	
		443.2		2782.2	5^-	
		841.3	100(5)	2384.2	6^-	
		1025.3	22.9(21)	2200.2	7^-	
3244.2	4^-	227.7		3016.4	5^-	
		1047.6	18(9)	2196.7	$(3)^+$	
		1246.5	22.2(21)	1997.7	4^+	
		1560.3	100(5)	1684.0	4^+	
		1903.6	92(4)	1340.5	3^+	
		2439.0	1.3(5)	803.1	2^+	
3260.4	6^+	1576.4	100	1684.0	4^+	
3279.2	5^-	35.0	0.11(1)	3244.2	4^-	
		262.7	19.3(3)	3016.4	5^-	
		339.9		2939.6	6^-	
		452.8	1.00(5)	2826.3	$(4)^-$	
		497.1[b]	97.8(10)	2782.2	5^-	
		895.1	100(1)	2384.2	6^-	
		1281.8	0.42(4)	1997.7	4^+	
		1595.3	32.0(4)	1684.0	4^+	
		2476.7	0.09(1)	803.1	2^+	
3328						
3377						
3402.7	5^-	620.5	18.1(2)	2782.2	5^-	Weak, not observed
		1018.6	23.8(3)	2384.2	6^-	transitions to 3279.2-
		1405.0	4.50(8)	1997.7	4^+	3244.2, 3016.4, 2939.6
		1718.7	100	1684.0	4^+	2826.3, 2647.8, 2200.2
						803.1-keV levels
3453	5^-					
3453.4	4^+	**2650.3**[b]	100	803.1	2^+	
3484.8		1699.5	54(14)	1784.1	2^+	
		2682.0[b]	100(18)	803.1	2^+	
3516	(4^+)	2713	100	803.1	2^+	
3562.9	5^-	1565.3	15.1(7)	1997.7	4^+	Weak, not observed
		1878.7	100(2)	1684.0	4^+	transitions to 3279.2,
						2782.2, 2647.8, and
						803.1-keV levels.
3606.2	2^+	957.9	64(13)	2647.8	3^-	
		1822.1[b]	100	1784.1	2^+	
3623	4^+					

[a] γ rays that were used for the construction of the total inelastic cross section.
[b] γ rays observed only in the first measurement due to better statistics.

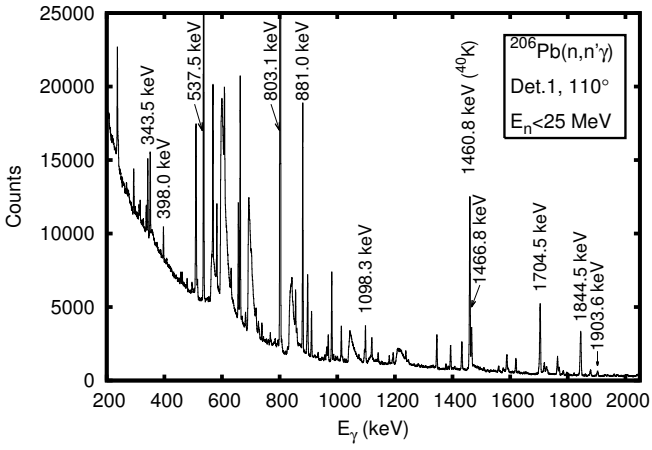

FIG. 1: γ ray spectrum recorded with a HPGe detector and with the ^{nat}Pb sample. The spectrum was integrated over neutron energies lower than ≈25 MeV. The main γ ray peaks from the inelastic scattering on ^{206}Pb are clearly visible.

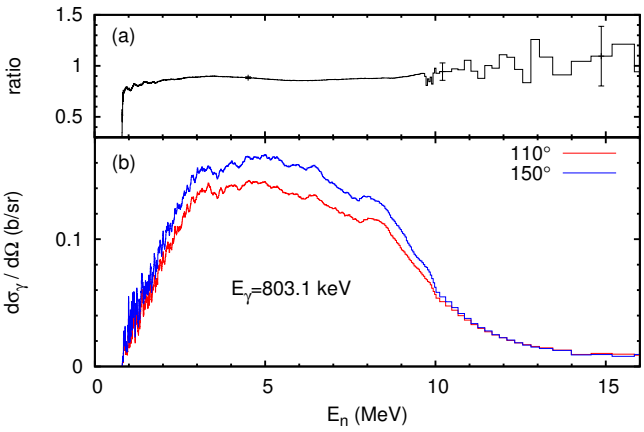

FIG. 2: (Color online) Differential γ production cross section for the 803.1-keV transition in ^{206}Pb at 110° and 150° together with the ratio between the differential cross section values. The present data were smoothed with an averaging moving window filter for an easier comparison

As in the cases of the ^{52}Cr [49] and ^{56}Fe [63] nuclei studied with the same experimental setup, well-defined resonance structures were observed for ^{206}Pb. The resonance structures in the differential and the integral γ production cross sections are shown in Fig. 3. The observation of these resonances was possible due to the very good neutron energy resolution. The results from two measurements agree very well [Fig. 3(b)].

In our previous studies [63, 64] we attempted an understanding of the structures observed in our cross sections by comparing the number of resonances directly counted with the theoretical level density estimated using the backshifted Fermi gas model formula parametrized in Ref. [65]. We concluded that for the first 0.5-1 MeV after the opening of the inelastic channel the structures may correspond to individual levels in the compound nucleus. However, above this range, the theoretical level density diverge severely from the number of resonances we can separate and therefore we considered that these resonances represent Ericson fluctuations. A similar estimate of the level density in ^{207}Pb results in very large numbers, of the order of a few hundred levels per MeV. From Fig. 3 it is clear that we do not see such a large number of resonances. We can state that in the case of ^{207}Pb, which is a much heavier nucleus then those previously studied, all structures we see in the cross sections are Ericson fluctuations.

Fig. 4 shows the integral γ production cross section of the 803.1-keV transition from the inelastic threshold up to 18 MeV. Only few experimental data points were found in the literature and significant discrepancies with most of these data are observed. The difference with the measured values of Lind *et al.* [15] increases with the increase of the incident neutron energy. The two data points of Lashuk *et al.* [66] and Yamamoto *et al.* [12] are very different compared with the present results: the first one lower and the second one, at about 15 MeV, is higher. The point value of Boring *et al.* [14] is also slightly higher than our result at about 3 MeV while the point measured by Day *et al.* [16] in the same energy region is in good agreement with our data.

The total uncertainty of the integral γ production cross section of the 803.1-keV γ ray is shown in Fig. 4(a). Uncertainty of about 5% was obtained below 9 MeV with a continuous increase above this energy. The increase of the uncertainties at the extremities of the measurement interval is due to the low counting rate (small cross sections and lower neutron flux at high energies) while the drop at E_n=10 MeV is due to a different binning of the time of flight spectra starting at that value.

Several TALYS calculations are shown in Fig. 4, using both default (black lines) and the microscopically-determined (blue lines) parameters. As discussed in the previous section dedicated to TALYS, the uncorrected calculations are shown using broken lines. The calculations corrected only for the branching ratio of the transition from the 0^+ level are shown using dotted lines. Those two lines are very close, showing that this correction does not play a significant role. The continuous lines display the fully-corrected TALYS calculations, i.e. calculations where also the correction for the isomeric level was applied. We note that all other TALYS calculations displayed through the current article include the two corrections discussed above.

2. *The 537.47-keV transition*

Fig. 6 shows the differential γ production cross section of the 537.5-keV M1+E2 transition from the first 3^+ level at 1340.5 keV to the 2^+ level at 803.1 keV.

The two measurements from the present experiment

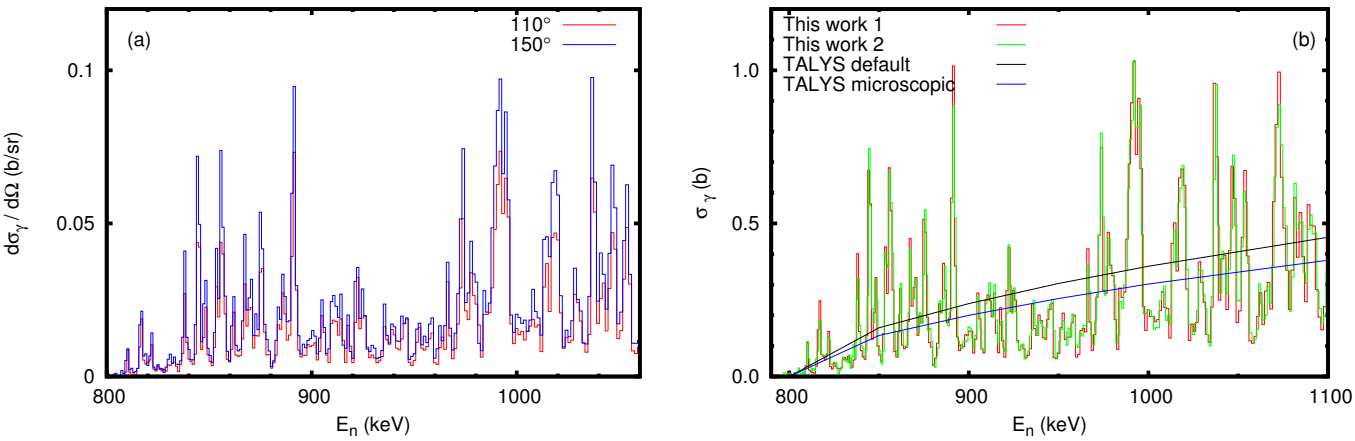

FIG. 3: (Color online) Full resolution γ production cross section for the 803.1 keV transition in ^{206}Pb: (a) Differential γ production cross section at 110° and 150°. (b) Integral γ production cross section compared with TALYS calculation.

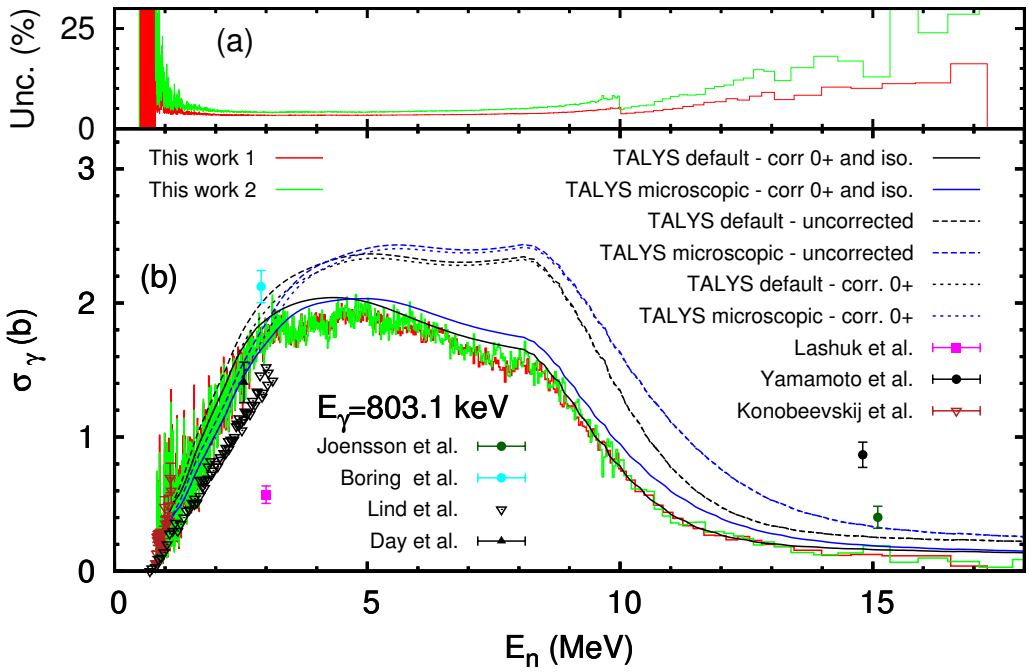

FIG. 4: (Color online) Integral γ production cross section for the 803.1 keV transition in ^{206}Pb. The upper panel represents the corresponding total uncertainty.

overlap. The experimental data of Lashuk *et al.* [67], Day *et al.* [16] and Lind *et al.* [67] are relatively close to the present results. The other two measurements (Boring *et al.* [14] and Yamamoto *et al.* [12]) are considerably higher. After the correction for the isomer, the TALYS calculation describes well the experimental data. A significant difference can still be observed between E_n=4 and 8 MeV where the calculation is higher. Even if the 537.5-keV transition is the result of the decay of third excited level, some resonance structures are still visible up to 1.7 MeV.

3. *Transitions from higher-lying levels*

Fig. 7 shows the integral γ production cross section for transitions from excited levels above 1466.8 keV. Up to E_x=2236.5 keV at least one γ ray was observed decaying

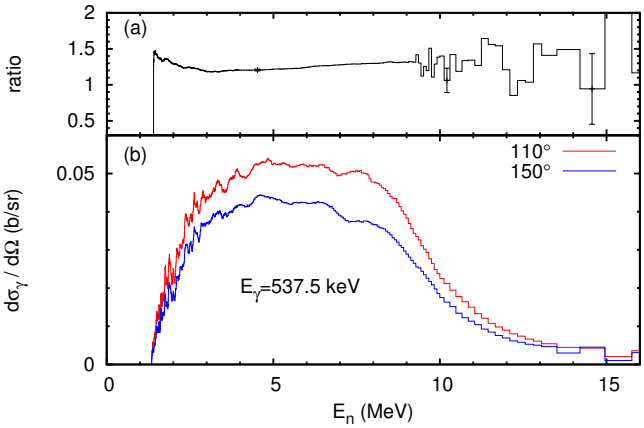

FIG. 5: Differential γ production cross section for the 537.5-keV transition in ^{206}Pb at 110° and 150° together with the ratio between the differential cross section values. The data were smoothed with an averaging moving window filter for an easier comparison

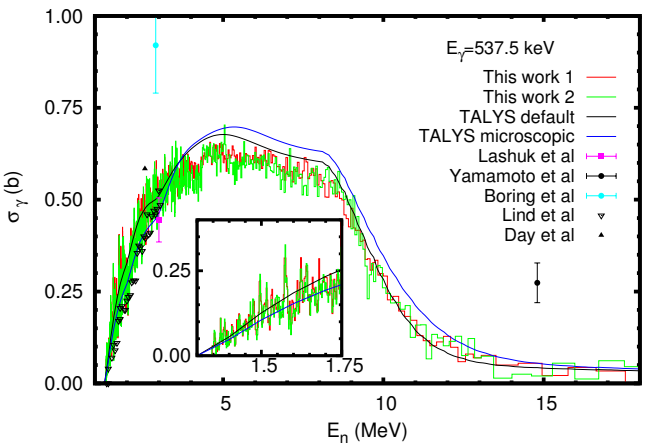

FIG. 6: Integral γ production cross section for the 537.5-keV transition in ^{206}Pb from threshold to E_n=18 MeV together with a zoom from the threshold up to 1.7 MeV, where resonance structure is still visible.

from each level. Above this energy some levels were not observed very probably because of their low cross section. The smaller γ production cross section determined in this experiment has a maximum of about 10 mb (the 956.6-keV transition).

The γ production cross section given for E_γ=1588 keV is a sum of the γ production cross sections of two transitions of 1588.2 and 1588.6 keV that decay from the levels at 2391.3 keV and at 2929.1 keV, respectively. The two γ rays could not be distinguished with the present experimental setup. However, from the threshold observed in the γ production cross section and from the comparison with TALYS (Fig. 7) it seems that the contribution from the γ decaying from the 2391.3-keV level is negligible.

The most intense γ ray from the level at 1466.8 keV (E_γ=663.8 keV) was not measured in the present experiment because of a background peak at about the same energy.

Only the measurements of Yamamoto *et al.* [12] for the 881.0 keV transition and Lind *et al.* [67] for the 1466.8- and 1704.5-keV γ rays were found in the literature (see Fig. 7). The Yamamoto *et al.* value for the production cross section of the 881.0 keV γ ray is much higher than the present results. The data of Lind *et al.* for the 1466.8- and the 1704.5-keV transitions agree well with the present measurement up to about 2.5 MeV. Above this energy, the Lind *et al.* data are higher.

All TALYS calculations were corrected for the decay from the isomer. The calculations using the microscopic input parameters describe better the transitions at 657.2, 1345.9, 856.6, and 1393.8 keV while the default parameters describe better the 718.9 and 956.6 keV transitions. The code strongly overestimates the 1433.5-keV transition. One can conclude that no clear systematic difference was observed between the calculation and the experimental data.

However, a general overview of the γ production cross sections and their comparison with the TALYS calculation reveals additional interesting information: In several cases the calculations are able to reproduce correctly the step-like features appearing in the shape of the excitation functions. This is the case for the steps observed at E_n ≈1.8 MeV in the cross sections of the 881.0- and 343.5-keV transitions decaying from the 1684.0-keV level. Such features of the γ production cross sections are probably caused by the excitation through the inelastic process of a level that further decays feeding the transition of interest: for E_n ≥1.8 MeV the two transitions mentioned above start to be fed also through the decay of the 2782.8- and 2826.3-keV levels, both strongly connected with the 1684.0-keV level. Nevertheless, similar features in the shape of other γ production cross sections are not correctly reproduced by TALYS. Clear examples are the 1704.5-, 981.0-, 1345.9- and 856.6-keV transitions which displaying step-like features around E_n=3-4 MeV. We interpret this disagreement as a sign of inconsistencies (possibly incorrect branching ratios or missing levels) in the level scheme of ^{206}Pb used by TALYS. Due to the remarkable lack of selectivity of the (n,n') reaction, the careful analysis of the excitation functions can therefore point out issues of the existing nuclear structure databases. Such a detailed analysis is, however, beyond the scope of the present article.

4. *Branching ratios*

In 5 cases, at least two γ rays from the decay of the same excited level in ^{206}Pb were observed with enough statistics to construct the γ production cross sections. For these levels it was possible to deduce the ratio between the γ ray intensities (branching ratios). These ra-

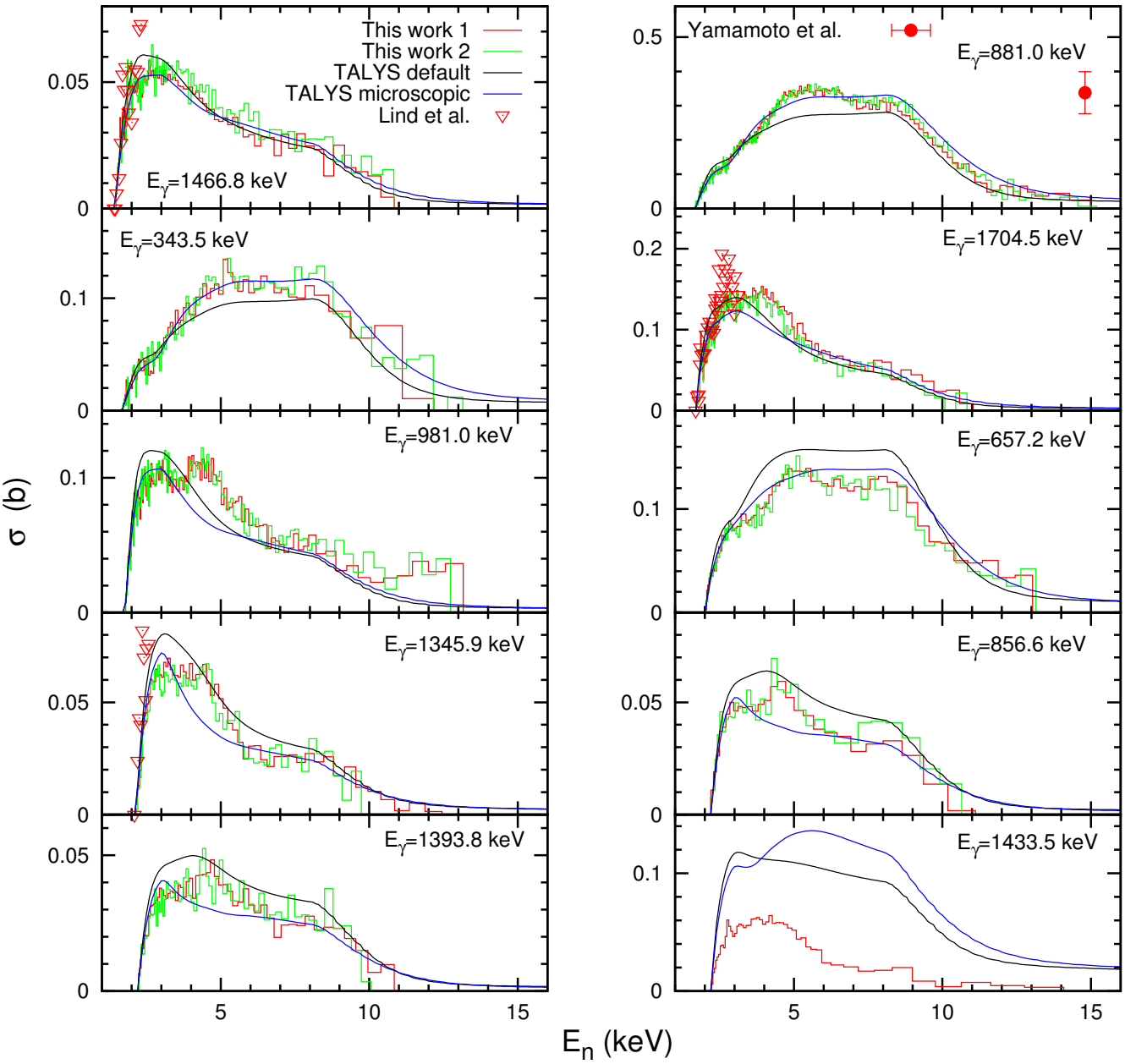

FIG. 7: (Color online) Integral γ production cross section for the transitions from higher lying levels in ^{206}Pb - 1/3.

tios were calculated from the corresponding γ production cross sections. The values presented in Table. III were deduced during the first measurement of the present work and were checked during the second one.

The measured thresholds of these γ rays agree with the calculated ones. As additional verification of the γ-ray identification, the present measured branching ratios are constant, within the uncertainties, as a function of the neutron energy. The present results agree reasonably with most of the evaluated values [37], significant differences being observed for the γ rays of 718.9 and 1246.5 keV.

5. *γ production cross sections from the (n, 2n) channel*

The threshold of the $(n, 2n)$ reaction on ^{206}Pb is at 8.13 MeV. The spectrum using the ^{nat}Pb sample integrated over neutron energies above the $(n, 2n)$ threshold is shown in Fig. 8. Although four transitions from ^{205}Pb are visible in this integrated spectrum, we could build the production cross sections only for the 703.4 and 987.7-keV γ rays, shown in Fig. 9. The observed experimental threshold of the $(n, 2n)$ transitions is the same as the theoretical value. The TALYS calculation overestimates the γ production cross section of both transitions, which could be related to the existence of an isomer in ^{205}Pb at

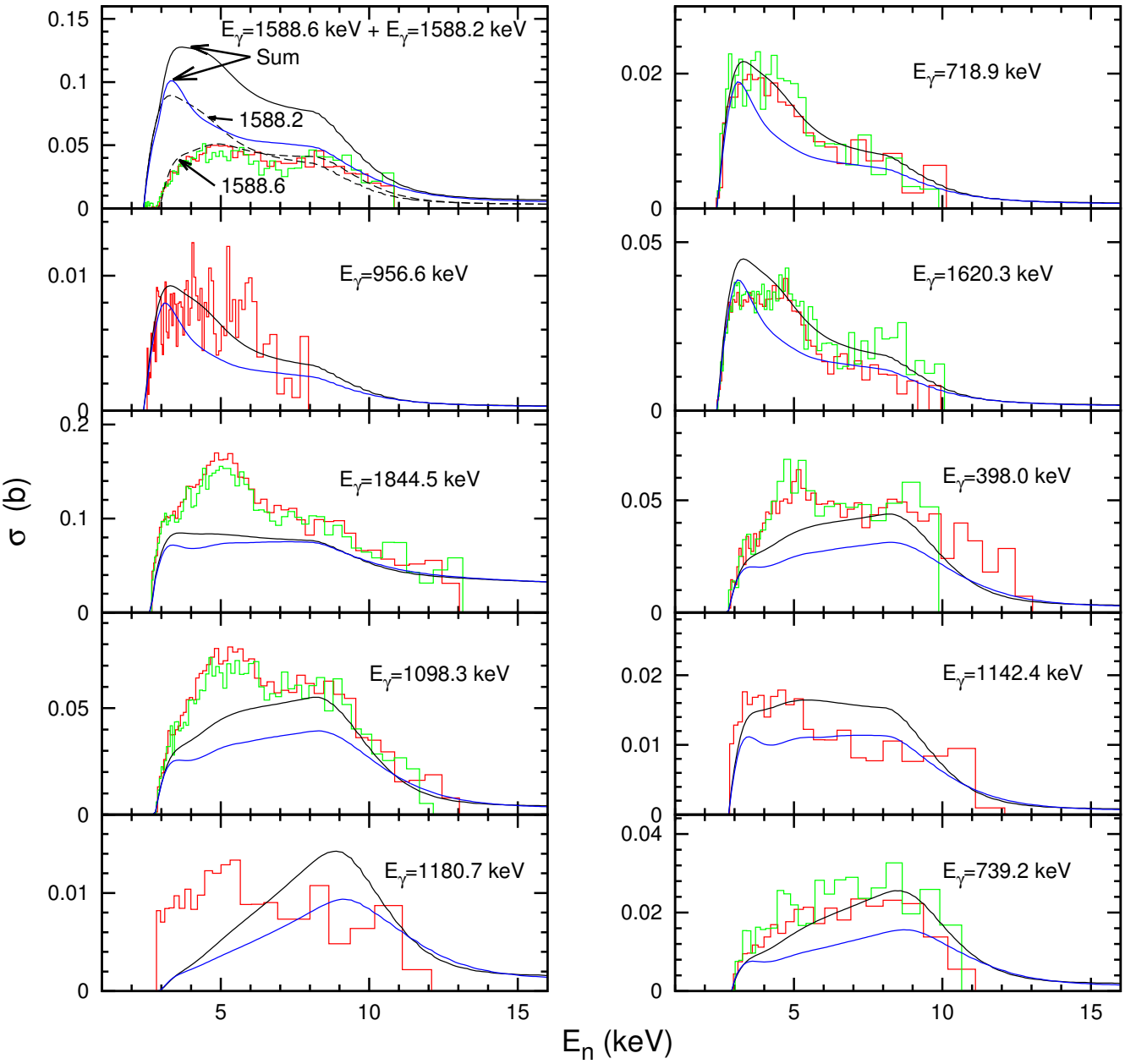

FIG. 7: (Color online) Integral γ production cross section for the transitions from higher lying levels in ^{206}Pb - 2/3.

1013.9 keV: we note that in this case the TALYS calculations were not corrected for the existence of this isomer.

B. Total inelastic and level cross sections

The total inelastic and level cross sections were constructed as described in Ref. [59] using the integral γ production cross sections and the evaluated level scheme of ^{206}Pb [37].

1. *Total neutron inelastic cross section*

For the construction of the total inelastic cross section we used the γ transitions with E$_\gamma$=803.1, 1466.8, 981.0, 1704.5 and 3194.6 keV (see Table. II). The total inelastic cross section so constructed does not include the contribution from the isomeric level at 2200.2 keV and from the 0^+ level at 1166.4 keV. According to the level scheme of ^{206}Pb, the first level that decays directly to the ground state and was not observed in the present experiment is at 3744.3 keV. This means that up to this energy the total inelastic cross section presented here is precise except

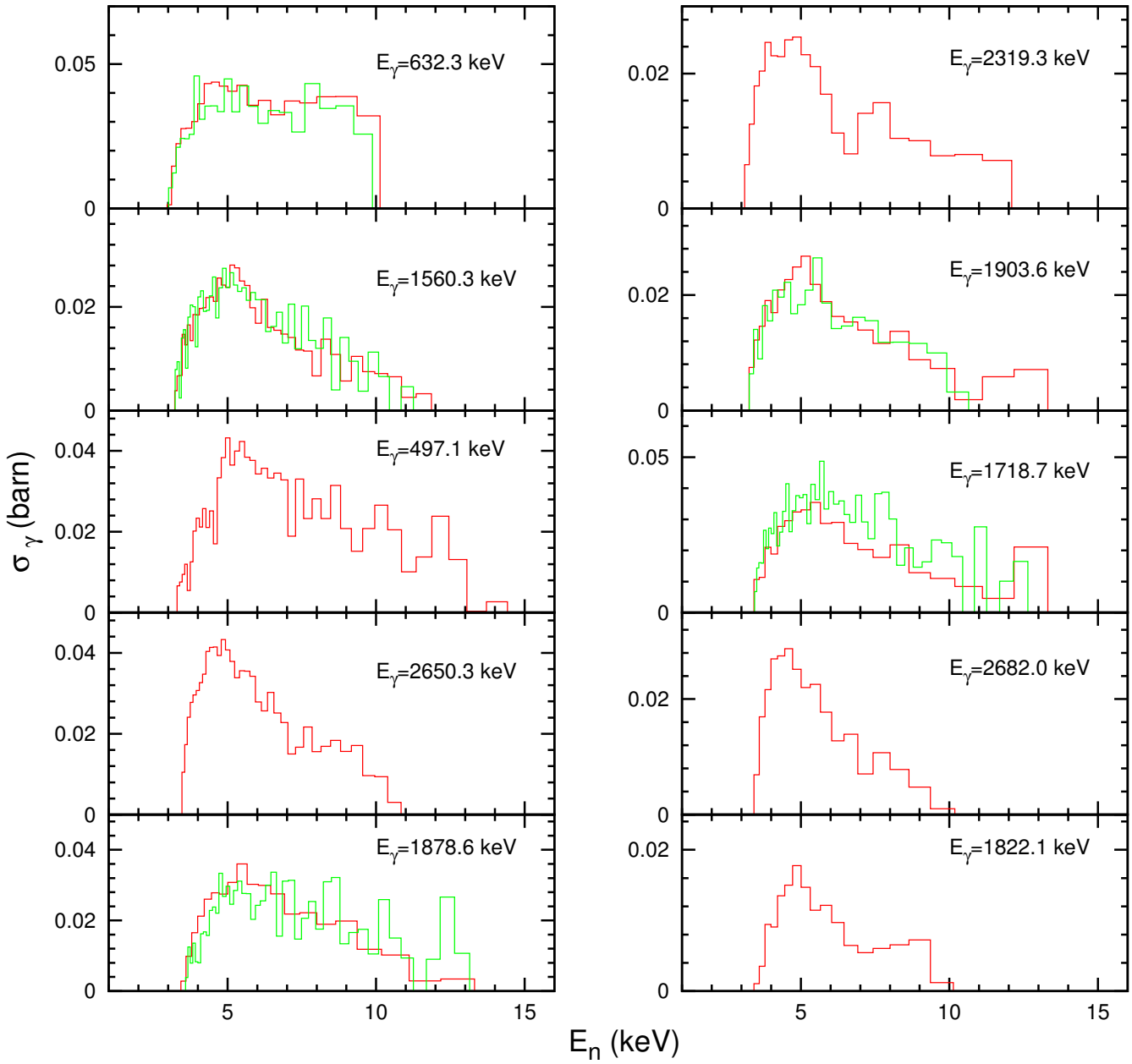

FIG. 7: (Color online) Integral γ production cross section for the transitions from higher lying levels in ^{206}Pb - 3/3.

for the contribution of the isomeric and of the 0^+ levels. Above E_n=3.762 MeV (which is the energy needed by a neutron in order to excite the 3744.3-keV level) the present curve is a low limit to the total inelastic cross section. However, this limit is a very close to the precise value for ^{206}Pb since in the present case most of the inelastic strength is collected through the first γ transition, which is by far the most intense from the spectrum.

The total inelastic cross section obtained in the first measurement of the present experiment is shown in Fig. 10 together with the corresponding total uncertainty. The total relative uncertainty is around 5% at $E_n \approx$2 MeV and increases slowly at higher energies. The large values of the relative total uncertainty at the extremities of the energy interval are due to the poor statistics and correspond to very low values of the cross section.

Several experimental points for the total inelastic cross sections found in the literature (Refs. [7, 8, 10, 16, 29, 31, 35]) are also displayed in Fig. 10. Our experimental data, with an uncertainty of the order of 5%, are much more precise than any previous measurement. We agree with the results of Landon *et al.* [8] and with Abdel *et al.* [67] in the low energy region, while the results of Holmqvist *et al.* [31], Thomson *et al.* [7] and Zafiratos *et al.* [35]

TABLE III: Branching ratios for levels in ^{206}Pb nucleus and the corresponding absolute uncertainties. The present results are compared with the values from the evaluated level scheme [37].

E_L(keV)	E_γ	Branching ratio	
		Present result	Evaluated ([37])
1684.0	343.5	37.3(7)	35.4(5)
	881.0	100	100.0(1)
2196.7	856.6	100	100
	1393.8	82.7(13)	78(5)
2423.4	718.92	63.5(21)	48.5(20)
	956.6	24.6(18)	20.6(16)
	1620.3	100	100(4)
2782.2	398.0	81.8(15)	79.6(7)
	1098.3	100	100(11)
3244.2	1246.5	36.9(37)	22.2(21)
	1560.3	100	100(5)
	1903.6	104.2(36)	92(4)

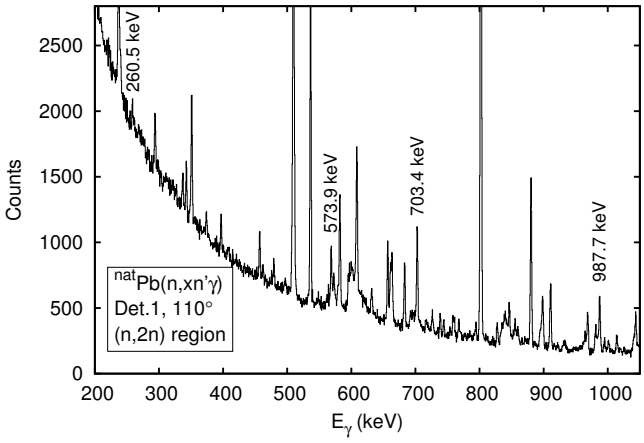

FIG. 8: γ spectrum with the ^{nat}Pb sample integrated over neutron energies above 8.12 MeV up to about 25 MeV. The 260.5, 573.9 and 703.4 and 987.7-keV peaks from the ^{206}Pb(n, 2n)^{205}Pb reaction are visible.

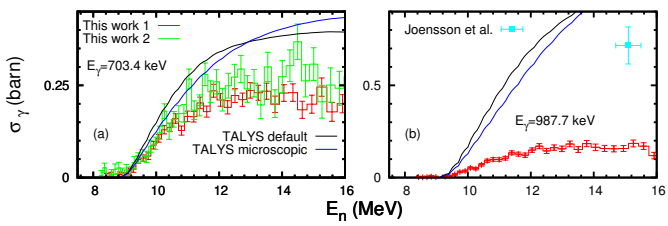

FIG. 9: Integral production cross section for the γ rays from the ^{206}Pb(n, 2nγ)^{205}Pb reaction.

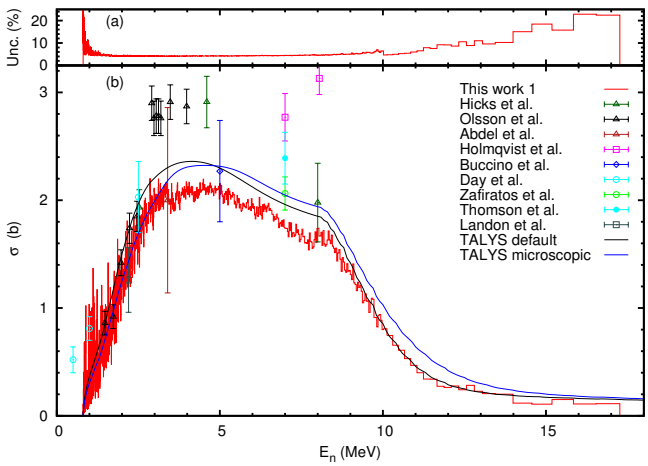

FIG. 10: Total neutron inelastic cross section of ^{206}Pb on full energy range up to 18 MeV. The upper panel represents the corresponding total uncertainty.

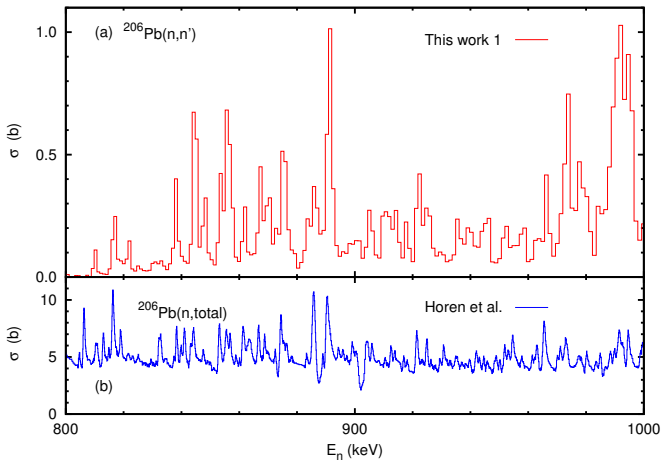

FIG. 11: Full resolution total inelastic cross section compared with the neutron total cross section measured at the Oak Ridge Electron Linear Accelerator [68] with a transmission setup.

at E$_n$=7 MeV are higher than our data (however, as already stated, at this neutron energy one should regard our result as a lower limit of the total inelastic cross section). Although a good overlap with the data of Olson *et al.* [29] exist at low neutron energies, our results start to diverge at energies around 3-4 MeV.

The TALYS calculation with default parameters describes well the present results after the correction for the isomer and for the E0 transition, especially at very high neutron energy. It seems that the microscopic calculation follows better the shape of the cross section at low energies but fails above E$_n$=3-4 MeV.

Fig. 11 compares the inelastic cross section below 1 MeV with the total neutron cross section measured at the Oak Ridge Electron Linear Accelerator in a transmis-

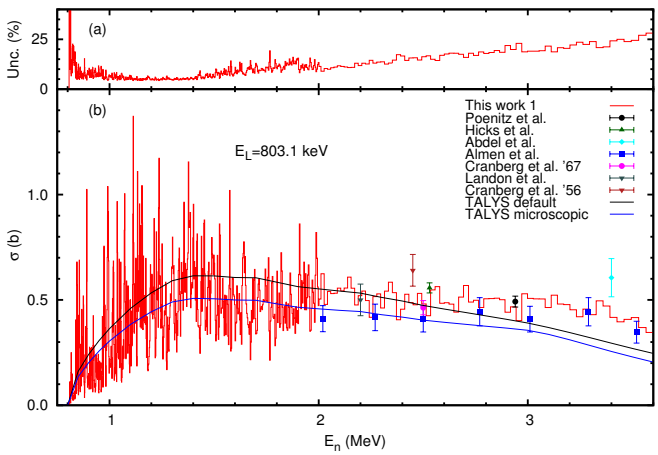

FIG. 12: The cross section of the 803.1-keV level in ^{206}Pb together with the corresponding total uncertainty.

sion experiment [68]. Despite the poorer neutron energy resolution of the present experiment, many of the resonances from the total cross section are seen also in the total inelastic cross section. Differences in the relative intensity between different resonances in the inelastic and in the total cross section exist. As an example, the two resonances at about 890 keV have almost the same intensity in the total cross section while in the inelastic cross section the resonance at 892 keV has higher intensity than the resonance at 886 keV. Also, we note that the absolute values of the inelastic cross section are a factor of ≈25 smaller than those of the total cross section (which includes the contributions from the elastic scattering - probably 50% - and from the capture - also significant).

2. *The 803.1-keV level*

The cross section of the first excited level is shown in Fig. 12. The first level not observed here that decays to the 803.1-keV level is at 2391.3 keV. Therefore, the cross section given here for the 803.1-keV level is precise up to 2.4 MeV. Above this energy, the curve from Fig. 12 is an upper limit for the 803.1 keV level cross section. The corresponding relative uncertainties are shown in Fig. 12(a).

The existing experimental data for this level cross section are mostly in good agreement with our result [4, 6, 8, 9]. The data of Almen *et al.* [67] are lower, but just at the limit of one standard deviation of the two experiments while those of Cranberg *et al.* [6] and Abdel *et al.* [67] seem slightly too high.

The TALYS calculation describes well the cross section of the level at 803.1 keV up to about 2.5 MeV. Above this energy, the calculation gives lower values. Part of this difference may come from the fact that the feeding from levels that were not observed above 2.4 MeV was neglected.

3. *Levels with higher excitation energy*

Fig. 13 shows cross sections of the levels with excitation energy between 1340.5 keV and 2647.8 keV. These cross sections were given only up to E_n=3.5 MeV because 3606.2 keV is the highest excited level observed in this experiment.

Above 2.3 MeV excitation energy some excited levels were not observed. Therefore, above E_n=2.3 MeV the level cross sections presented here should be considered as upper limits of the exact values. The difference to the exact values reflects the intensity of the excited levels not observed in this experiment. The cross section of these levels has to be weak such as the transitions that decay from them to have a cross section of less than 10 mb, which is the approximate observation limit of the present measurement.

Previous experimental results were found for several levels. The data of Almen *et al.* [67] for the 1340.5 keV level are slightly too low but those for the 1466.8-keV level overlap perfectly with ours. At E_n=2.5 MeV Cranberg *et al.* [6] display results that agree also with ours rather well.

TALYS calculations using default and microscopic input parameters are plotted together with the present results (Fig. 13). Below 2.3 MeV neutron energy, the agreement between the calculation and the present measurement is good for the majority of the levels presented here. Above 2.5 MeV, the calculation gives lower values than the present measurement for the levels at 1340.5, 1684.0, and 2647.8 keV. These differences confirm our interpretation of the present results as lower limits of the cross sections above 2.3 MeV. Finally, we note that the agreement with TALYS seems to improve in several cases when the microscopic parameters are used.

V. CONCLUSIONS

The neutron inelastic and the $(n, 2n\gamma)$ cross sections on ^{206}Pb were measured with an unprecedented neutron energy resolution from threshold up to E_n=18 MeV. Two measurements were performed using different samples and different acquisition systems and the very good agreement between the two measurements increased the confidence in the results. The good resolution of the HPGe detectors allowed the identification of 34 γ rays from the inelastic channel and 2 γ rays from the $(n, 2n\gamma)$ channel. Angle-integrated γ production cross sections were determined for all these transitions. The total uncertainty for the most intense transition was about 5% below 9 MeV. The maximum observed excitation energy was 3.6 MeV for the inelastic scattering. A neutron energy resolution of 1.1 keV at 1 MeV allowed the observation of resonant structures for the first time in the inelastic scattering on ^{206}Pb up to E_n ≈1.7 MeV. However, a comparison of the number of resonance-like structures observed with the estimated level density in ^{207}Pb around

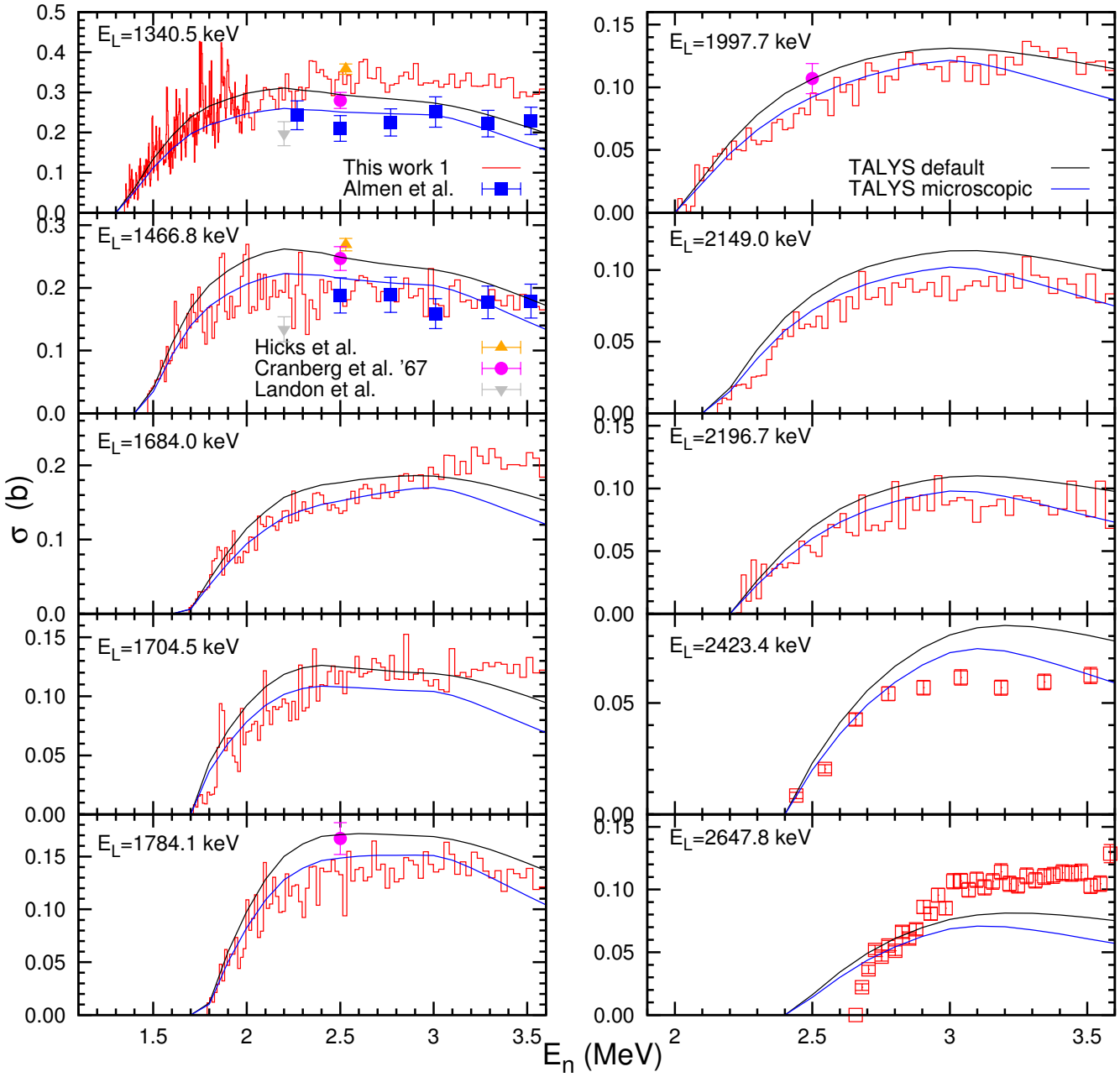

FIG. 13: The cross section of the excited levels above 1.3 MeV in ^{206}Pb.

the excitation energy $S_n + E_n$ suggests that these structures represent only Ericson fluctuations.

In several cases, we were able to infer, based on our γ production cross sections, new branching ratios. These are mostly in good agreement with the existing evaluated values.

The total inelastic and the level cross section were constructed relying on the present evaluated level scheme of ^{206}Pb and using the angle-integrated γ production cross sections. The level cross sections are precise up to 2.3 MeV while above this threshold they represent upper limits. The total inelastic cross section determined here does not include the contribution from the isomer level at 2200.2 keV and from the 0^+ level at 1166.4 keV. Except these, our result for the total inelastic cross section is accurate up to 3.2 MeV; above this energy it is only a lower limit to the total inelastic cross section.

The present results were compared with existing experimental data found in the literature and with calculations performed with the version 1.6 of the TALYS code. The theoretical calculations were performed using default parameters but also a set of microscopically determined parameters. There is a good overall agreement between the present data and the calculations, mainly due to the optical model parameters which are known well in the mass region of the lead isotopes. Moreover, no clear im-

provement was obtained by using microscopically determined parameters. Finally, we note that the comparison between the shape of several experimental γ production cross sections and the corresponding TALYS calculations seems to indicate possible deficiencies in the level scheme of ^{206}Pb.

Acknowledgments

The authors thank the team of GELINA operators for the quality of the neutron beam, A. Moens and C. Quétel for preparation and characterization of the sample, and R. Wynants for technical support. A.N., L.C.M. and C.B. are grateful to IRMM for financial support. This work was partially supported by the European Commission within the Sixth Framework Programme through the EUROTRANS (EURATOM contract number 516520) and EFNUDAT (EURATOM contract number 036434) projects and within the Seventh Framework Programme through the CHANDA project (EURATOM contract number FP7-605203).

[1] G. Aliberti, G. Palmiotti, M. Salvatores, and C.G. Stenberg, Nucl. Sci. Eng. 146, 13 (2004).
[2] G. Aliberti *et al.*, Ann. Nucl. Energy 33, 700 (2006).
[3] M. Salvatores (coordinator) and R. Jacqmin (monitor), NEA/WPEC-26 report, volume 26, ISBN 978-92-64-99053-1, 2008.
[4] S. Hicks, J. Hanly, S. Hicks, G. Shen, and M. McEllistrem, Phys. Rev. C49, 103 (1994).
[5] E. Almén-Ramström, Report AE-503, Aktiebolaget Atomenergie, Studsvik, Nyköping, Sweden (1975).
[6] L. Cranberg, T. A. Oliphant, J. Levin, and C. D. Zafiratos, Phys. Rev. 159, 969 (1967).
[7] D. Thomson, Phys. Rev. 129, 1649 (1963).
[8] H.H. Landon, A.J. Elwyn, G.N. Glasoe, and S. Oleksa, Phys. Rev. 112, 1192 (1958).
[9] E. Poenitz, R. Nolte, D. Schmidt, and G. Chen, J. Korean Phys. Soc 59, 1876 (2011).
[10] S.G. Buccino, C.E. Hollandsworth, H.W. Lewis, P.R. Bevington, Nucl. Phys. 60, 17 (1964).
[11] J.K. Dickens, Phys. Rev. C28, 916 (1983).
[12] T. Yamamoto, Y. Hino, S. Itagaki, and K. Sugiyama, J. of Nucl. Sci. and Tech. 15, 797 (1978).
[13] B. Jönsson, K. Nyberg, and I. Bergqvist, Arkiv för Fysik 39, 295 (1968).
[14] J.W. Boring and M.T. McEllistrem, Phys. Rev. 124, 1531 (1961).
[15] D.A. Lind and R.B. Day, Ann. Phys. 12, 485 (1961).
[16] R.B. Day, Phys. Rev. 102, 767 (1956).
[17] R.M. Kiehn and C. Goodman, Phys. Rev. 95, 989 (1954).
[18] G.N. Salaita and P.K. Eapen, J. Inorg. Nucl. Chem. 35, 2139 (1973).
[19] K.C. Garg, C.S. Khurana, Indian J. Pure Appl. Phys. 17, 525 (1979).
[20] J. Fréhaut, A. Bertin, R. Bois, and J. Jary, in: Symposium on Neutron Cross Sections from 10-50 MeV, BNL-NNDC, Upton N.Y., U.S.A, 1980.
[21] D.J. Horen, J.A. Harvey, and N.W. Hill, Phys. Rev. C20, 478 (1979).
[22] B.A. Benetskij, A.B. Kljachko, V.V. Nefjodov, and I.M. Frank, I.V. Shtranikh, Yad. Fyz. 17, 21 (1973).
[23] D.G. Foster Jr. and D.W. Glasgow, Phys. Rev. C3, 576 (1971).
[24] A.D. Carlson and H.H. Barschall, Phys. Rev. 158, 1142 (1967).
[25] J.V. Dukarevich, A.N. Djumin, and D.M. Kaminker, Nucl. Phys. A92, 433 (1967).
[26] G.M. Haas and P.L. Okhuysen, Phys. Rev. 132, 1211 (1963).
[27] J.H. Coon, E.R. Graves, and H.H. Barschall, Phys. Rev. 88, 562 (1952).
[28] D.W. Miller, R.K. Adair, C.K. Bockelman, and S.E. Darden, Phys. Rev. 88, 83 (1952).
[29] N. Olsson, B. Holmqvist, and E. Ramström, Nucl. Phys. A385, 285 (1982).
[30] J.C. Ferrer, J.D. Carlson, and J. Rapaport, Nucl. Phys. A275, 325 (1977).
[31] B. Holmqvist and T. Wiedling, Report AE-482, Aktiebolaget Atomenergie, Studsvik, Nyköping, Sweden (1973).
[32] G.E. Belovitskij, L.N. Kolesnikova, and I.M. Frank, Yad. Fyz. 15, 662 (1972).
[33] B. Holmqvist and T. Wiedling, Report AE-430, Aktiebolaget Atomenergie, Studsvik, Nyköping, Sweden (1971).
[34] S.G. Buccino, C.E. Hollandsworth, and P.R. Bevington, Z. Phys. 196, 103 (1966).
[35] C.D. Zafiratos, T.A. Oliphant, J.S. Levin, and L. Cranberg, Phys. Rev. Lett. 14, 913 (1965).
[36] A.D. Carlson *et al.*, Nucl. Data Sheets 110, 3215 (2009).
[37] F. G. Kondev, Nucl. Data Sheets 109, 1527 (2008).
[38] A.J. Koning and J.P. Delaroche, Nucl. Phys. A713, 231 (2003).
[39] A.J. Koning and M.C. Duijvestijn, Nucl. Phys. A744, 15 (2004).
[40] A.J. Koning, S. Hilaire, S. Goriely, Nucl. Phys. A810, 13 (2008).
[41] R. Capote *et al.*, Nucl. Data Sheets 110, 3107 (2009).
[42] E. Bauge, J. Delaroche, and M. Girod, Phys. Rev. C58, 1118, (1998).
[43] E. Bauge, J. Delaroche, and M. Girod, Phys. Rev. C63, 024607 (2001).
[44] S. Hilaire and S. Goriely, Nucl. Phys. A779, 63 (2006).
[45] S. Goriely, S. Hilaire, and A.J. Koning, Phys. Rev. C78, 064307 (2008).
[46] A.J. Koning, M.C. Duijvestijn, Nucl. Instrum. Meth. Phys. Res. B248, 197 (2006).
[47] A.J. Koning and D. Rochman, Nucl. Data Sheets 113, 2841 (2012).
[48] L.C. Mihailescu, L. Oláh, C. Borcea, and A. J. M. Plompen, Nucl. Instrum. Meth. Phys. Res. A531, 375 (2004).
[49] L. Mihailescu, C. Borcea, A. Koning, and A. Plompen, Nucl. Phys. A786,1 (2007).
[50] L.C. Mihailescu, C. Borcea, and A. Plompen, Nucl. Instrum. Meth. Phys. Res. A578, 298 (2007).

[51] D. Ene, C. Borcea, S. Kopecky, W. Mondelaers, A. Negret, and A. Plompen, Nucl. Instrum. Meth. Phys. Res. A493, 106 (2002).
[52] M. Flaska, A. Borella, D. Lathouwers, L.C. Mihailescu, W. Mondelaers, A.J.M. Plompen, H. van Dam, and T.H.J.J. van der Hagen, Nucl. Instrum. Meth. Phys. Res. A531, 392 (2004).
[53] D. Tronc, J.M. Salomé, and K. Böckhoff, Nucl. Instrum. Meth. Phys. Res. A228, 217 (1985).
[54] J. F. Briesmeister, Report LA-13709-M, Los Alamos National Laboratory, Los Alamos NM, USA (2000).
[55] D. Deleanu, C. Borcea, P. Dessagne, M. Kerveno, A. Negret, A.J.M. Plompen, and J.C. Thiry, Methods Phys. Res. A624, 130 (2010).
[56] L. C. Mihailescu, Report EUR 22343 EN, ISBN 92-79-02885-5, ISSN 1018-5593, European Communities (2006).
[57] R. Nolte and D.J Thomas, Metrologia 48, S274 (2011).
[58] A. Plompen *et al.* J. Korean Phys. Soc 59, 1581 (2011).
[59] C. Rouki, P. Archier, C. Borcea, C. De Saint Jean, J.C. Drohé, S. Kopecky, A. Moens, N. Nankov, A. Negret, G. Noguère, A.J.M. Plompen, and M. Stanoiu, Nucl. Instrum. Meth. Phys. Res. A672, 82 (2012).
[60] A.J. Koning, S. Hilaire, and M.C. Duijvestijn, Proc. Int. Conf. on Nuclear Data for Science and Technology - ND2004, Sep. 26 - Oct. 1, 2004, Santa Fe, USA, AIP Conference proceedings 769, Melville, NY, p.1154 (2005).
[61] J. Raynal, Tech. Rep. CEA-N-2772, CEA, Saclay, France (1994).
[62] E. Sheldon and V. C. Rogers, Comp. Phys. Comm. 6, 99 (1973).
[63] A. Negret, C. Borcea, Ph. Dessagne, M. Kerveno, A. Olacel, A.J.M. Plompen, and M. Stanoiu, Phys. Rev. C90, 034602 (2014).
[64] A. Olacel, C. Borcea, Ph. Dessagne, M. Kerveno, A. Negret, and A.J.M. Plompen, Phys. Rev. C90, 034603 (2014).
[65] T. von Egidi and D. Bucurescu, Phys. Rev. C72, 044311 (2005).
[66] A.I. Lashuk and I.P. Sadokhin, Yad. Konst. 2, 59 (1996).
[67] EXFOR, Nuclear reaction data, www.nndc.bnl.gov (CSISRS), www.nea.fr/html/dbdata/x4/x4ret.html or www-nds.iaea.or.at/exfor (2006).
[68] D.J. Horen, J.A. Harvey, and N.W. Hill, Phys. Rev. C24, 1961 (1981).